Evaluation of the tensile and fatigue behaviour of ingot metallurgy beryllium/aluminium alloys

V. C. NARDONE, T. J. GAROSSHEN
United Technologies Research Center, East Hartford, CT 06108, USA

The tensile and fatigue behaviour of ingot metallurgy beryllium/aluminium alloys produced by Nuclear Metals, Inc., is determined as a function of temperature. The wrought alloy and the casting alloy are both shown to have a very high stiffness to density ratio compared with common structural materials. The wrought alloy was found to have superior fatigue strength, tensile strength and ductility relative to the casting alloy; it also maintained a greater fraction of its tensile strength as a function of temperature. The stiffness of the materials can be readily explained using standard composite theory, where the material is treated as a discontinuous beryllium-reinforced aluminium matrix composite. The strength of the casting alloy is controlled to a large extent by the strength of its aluminium alloy matrix. In contrast, strengthening increments from both dislocation-based mechanisms and load transfer appear to be operative for the wrought material. Fractographic analysis of tensile specimens showed that preferential failure of the aluminium regions or the beryllium/aluminium interfacial regions occurs under certain circumstances. Fracture analysis of fatigue samples revealed no obvious fracture initiation sites and no evidence of limited/controlled crack growth regions.

1. Introduction

There continues to be a need for high-performance low-density materials in aerospace applications. One class of material currently under development for such applications is the beryllium–aluminium alloys being marketed by Nuclear Metals, Inc. (NMI), under the tradename Beralcast®. The Beralcast alloys consist of 65 wt % Be with the balance being an aluminium alloy matrix. The composition of the aluminium alloy matrix is tailored to result in a material that is suitable for use as either an investment casting alloy or a wrought alloy suitable for extrusion. Because beryllium is virtually insoluble in aluminium, essentially pure primary beryllium dendrites form during the solidification of the Beralcast alloys. The resulting microstructure consists of a bi-metallic structure of pure beryllium particles contained within an aluminium alloy matrix. The presence of the aluminium regions in the Beralcast alloys results in substantially improved ductility and fabricability relative to pure beryllium.

The purpose of this work was to evaluate the mechanical properties of two different alloys produced by NMI: the casting alloy Beralcast 363 and the wrought alloy Beralcast 310. Specifically, both the tensile and fatigue performance of the Beralcast alloys are determined as a function of temperature. To date, only the room-temperature tensile properties of these materials have been published [1]. In addition, a microstructural and failure mode analysis was performed to complement the mechanical property testing to help establish the microstructure/property relationships that exist for these unique materials.

2. Experimental procedure

2.1. Material

The Beralcast alloys were received from NMI in two different forms. The casting alloy Beralcast 363 was produced as 1.27 cm (0.50 in.) outer diameter (o.d.) investment cast segments that were machined to final dimensions. The wrought alloy Beralcast 310 was produced in the form of a 1.27 cm (0.50 in.) o.d. extruded rod approximately 1.5 m (5 ft) in length. Both materials were tested in the as-fabricated condition. Optical micrographs of the Beralcast materials are shown in Figs 1–3. The beryllium phase, which constitutes $\sim 73\%$ of the material by volume, appears dark in the micrographs. This beryllium volume fraction level results in a material density of $2.12\,g\,cm^{-3}$ ($0.076\,lb/in^{-3}$) for both of the alloys. The nominal alloy compositions (wt %) are Al–65Be–3Ag–1Ge –1Co for the Beralcast 363 alloy and Al–65Be–2Ag –2Si for the Beralcast 310 alloy. The compositions have been tailored by NMI to result in a material that has good mechanical properties and adequate castability (for the cast product) and formability (for the wrought product) [1]. Note that the alloying additions segregate to the aluminium regions of the material such that the materials essentially consist of pure beryllium regions that are embedded within an aluminium alloy matrix [1].

The microstructure of the casting alloy shown in Fig. 1 is representative of samples taken from multiple orientations, i.e. there was no directionality in the material's microstructure. Note that the cast material has a coarse microstructure, with the width of the

0022–2461 © *1997 Chapman & Hall*

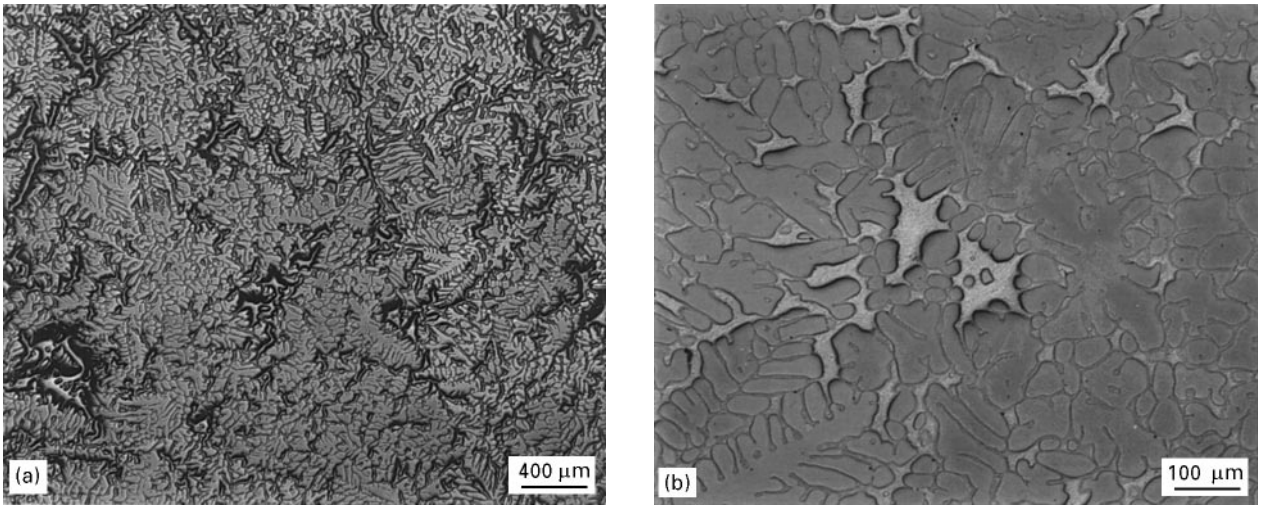

Figure 1 (a, b) Cross-sections of the Beralcast 363 casting alloy.

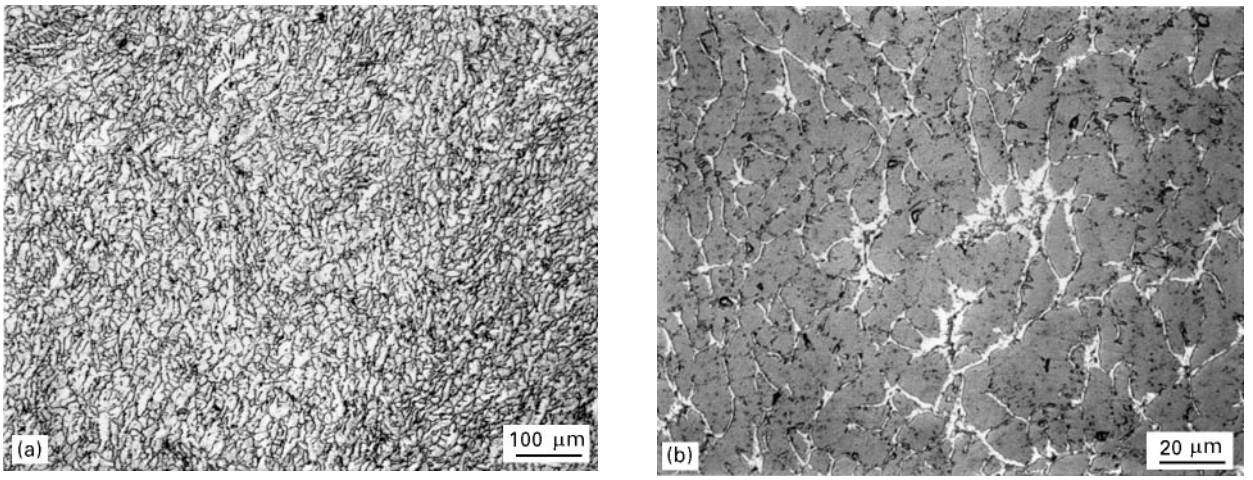

Figure 2 (a, b) Cross-sections of the Beralcast 310 extruded rod (etched for improved contrast).

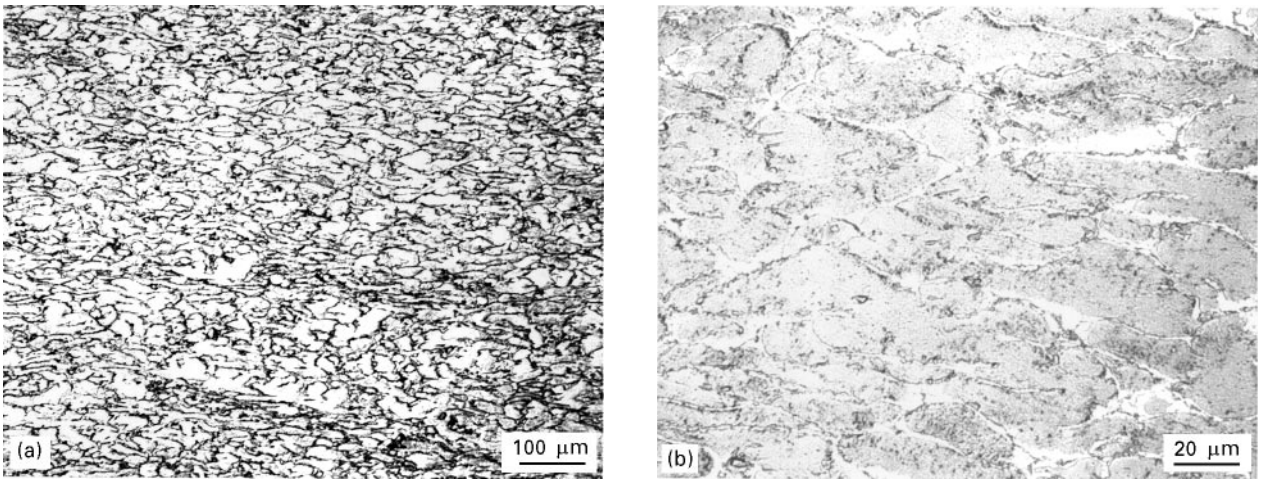

Figure 3 (a, b) Longitudinal sections of the Beralcast 310 extruded rod (etched for improved contrast).

secondary beryllium dendritic arms being approximately 50 μm in size. The length of the dendritic arms is typically about 100 μm, while the primary dendritic cores are several hundred micrometres in length. Although the beryllium regions are irregular in shape, they do have an appreciable aspect ratio. The spacing between the beryllium regions is typically on the order of tens of micrometres.

Optical micrographs of the microstructure of the extruded material is shown in Figs 2 and 3. In this case, the extrusion process aligns the beryllium regions along the extrusion direction. This may be

observed by comparing the longitudinal section shown in Fig. 2 with the transverse section shown in Fig. 3. The microstructure in the wrought product is also more refined relative to the cast product. The typical width of the beryllium regions is from 10–20 μm, with the typical spacing between the beryllium regions being about 2 μm. The transverse section of Fig. 3 indicates that the beryllium regions have a typical aspect ratio of about 8 to 1.

2.2. Procedure

Both tensile and fatigue properties were determined for the Beralcast alloys. The tensile testing was conducted at room temperature, 232 °C (450 °F) and 371 °C (700 °F) for as-cast Beralcast 363 samples and for the longitudinal (parallel to the extrusion direction) orientation of the Beralcast 310 rod. The tensile test specimen had a nominal 0.61 cm (0.24 in.) gauge diameter by 3.8 cm (1.5 in.) gauge length with threaded end attachment regions. The tensile testing was conducted at a constant crosshead displacement rate of 0.13 cm min^{-1} (0.05 in. min^{-1}). Extensometry having a 2.54 cm (1.0 in.) gauge length was used to measure the sample strain.

All of the fatigue testing was conducted at 232 °C (450 °F) and an R value (ratio of minimum to maximum stress) of 0.1. Smooth cylindrical constant gauge section samples with threaded end regions were used for the fatigue testing. The samples of the cast material had a 0.46 cm (0.18 in.) gauge diameter, while the samples of the wrought material had a 0.64 cm (0.25 in.) gauge diameter. The testing was performed at frequencies ranging from 5–20 Hz, where the higher frequencies were used for the lower load levels.

Scanning electron microscopy (SEM) was performed on failed tensile and fatigue samples to assess the microstructural factors that influence material performance.

3. Results

3.1. Tensile test results and fractographic analysis

A summary of the tensile test results is provided in Table I, while stress–strain curves as a function of temperature are shown in Figs 4 and 5. As might be

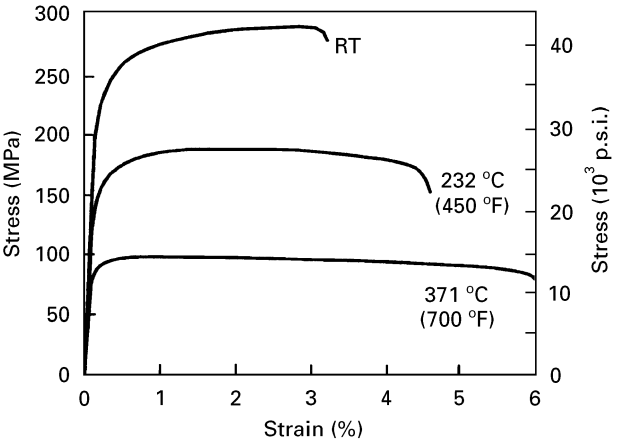

Figure 4 Stress–strain curves as a function of temperature for the cast Beralcast material.

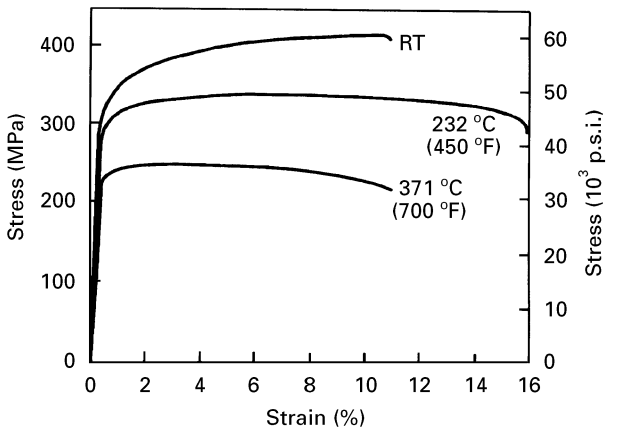

Figure 5 Stress–strain curves as a function of temperature for the extruded Beralcast material.

TABLE I Tensile test results

Temp.		Elastic modulus		Yield strength		Tensile strength		Failure strain
(°C)	(°F)	(GPa)	(10^6 p.s.i.)	(MPa)	(10^3 p.s.i.)	(MPa)	(10^3 p.s.i.)	(%)
Beralcast 363–casting alloy								
Room temp.		218	31.6	249	36.1	290	42.0	3.3
		244	35.4	216	31.3	264	38.3	1.8
232	450	176	25.5	163	23.9	184	26.7	5.2
		168	24.4	165	23.9	190	27.6	4.5
371	700	134	19.4	95	13.7	99	14.4	6.2
		152	22.0	71	10.3	77	11.2	9.3
Beralcast 310–wrought alloy								
Room temp.		238	34.6	293	42.4	421	61.0	14.8
		238	34.6	295	42.8	421	61.0	9.9
232	450	197	28.6	286	41.5	343	49.7	16.7
		184	26.7	287	41.6	343	49.7	16.6
371	700	136	27.0	241	35.0	275	39.9	6.5
		169	24.5	222	32.2	250	36.2	10.9

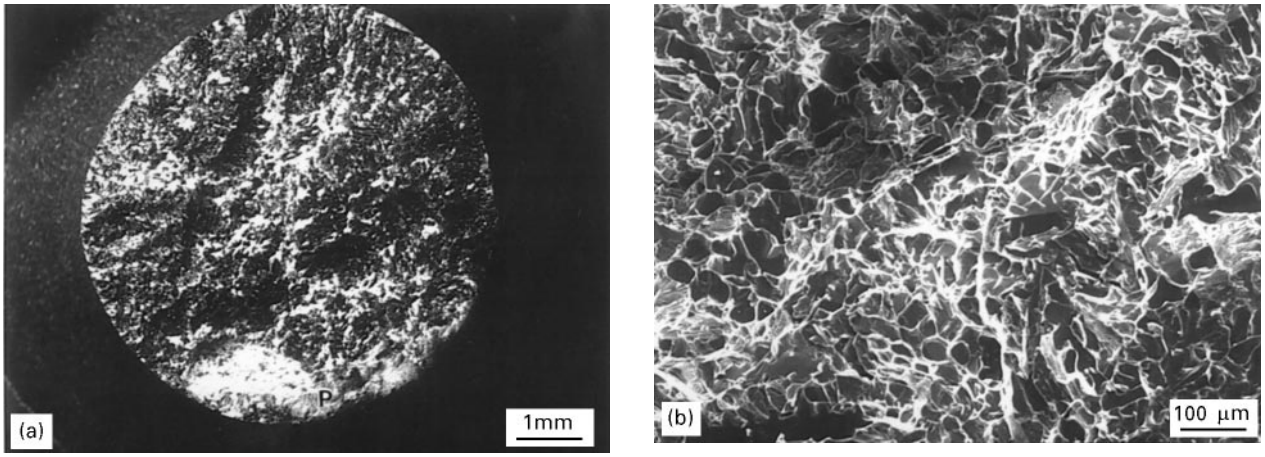

Figure 6 (a, b) SEM images of room-temperature tensile fracture surface of the cast material.

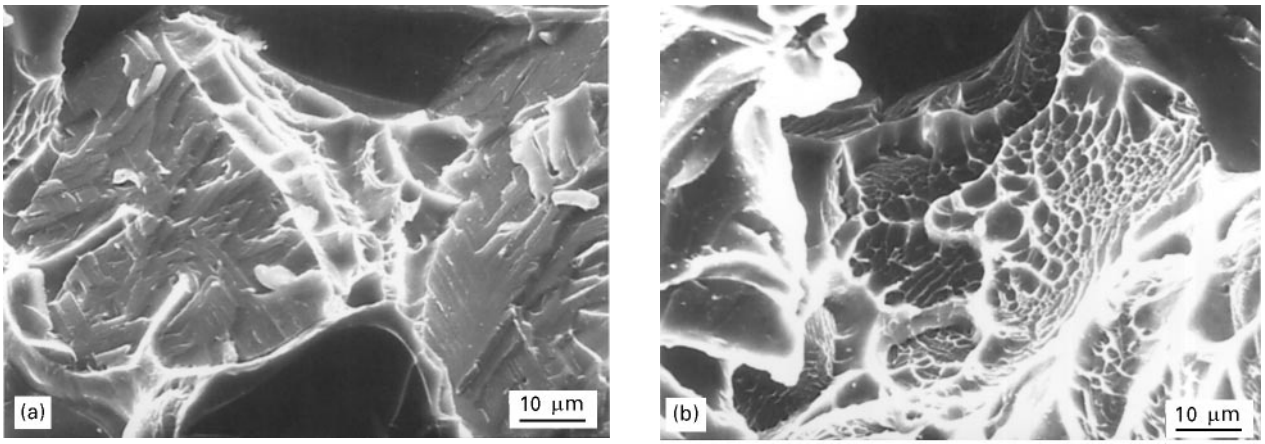

Figure 7 High-magnification scanning electron micrographs of the room-temperature tensile fracture of the cast material. (a) Beryllium cleavage fracture, (b) aluminium ductile dimple failure.

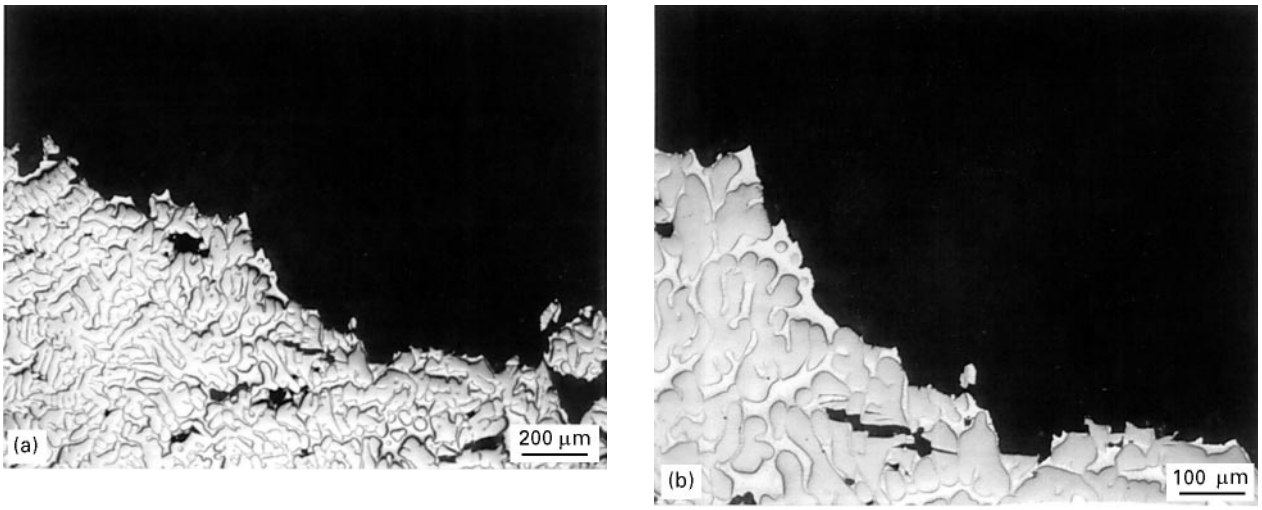

Figure 8 (a, b) Longitudinal sections through the fracture surface for a room-temperature tensile specimen of the cast material.

expected, the results indicate that the wrought product possess superior strength and ductility relative to the cast product. In particular, the wrought product shows a substantial amount of plasticity in the stress–strain curves. The wrought product also maintains a greater fraction of its room-temperature strength as a function of temperature.

Illustrations of the tensile fracture surfaces for both the cast and wrought materials as a function of temperature are shown in Figs 6–13. The appearance of the fracture surface for the cast material did not vary as a function of temperature. Therefore, the results presented in Figs 6 and 7 for the room-temperature sample are also representative of the elevated-temperature samples. The fracture surfaces of the cast samples tend to have a relatively non-planar, rough morphology. At higher magnifications, ductile dimple fracture of the aluminium regions and a cleavage-type fracture for the beryllium regions, is observed.

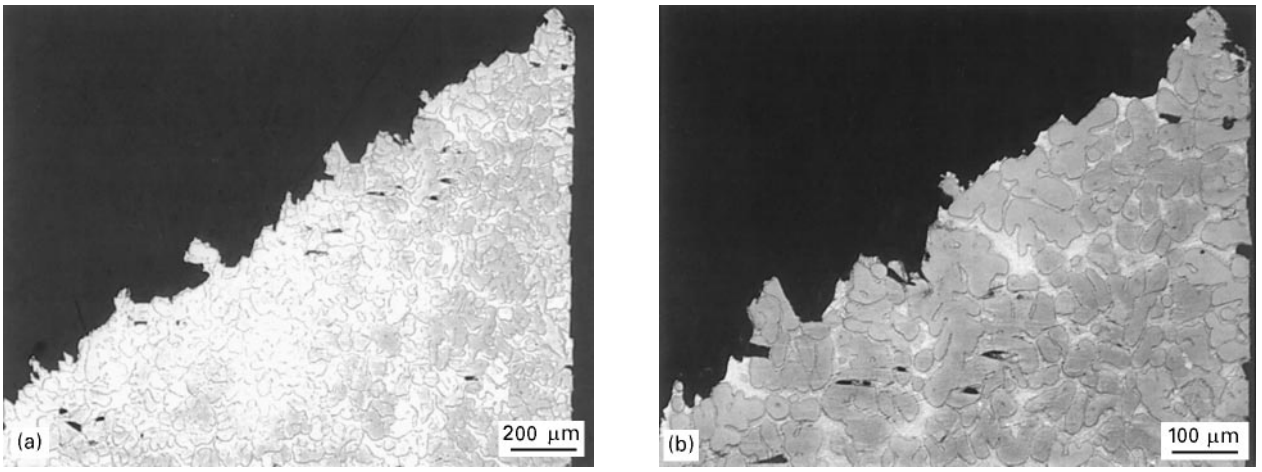

Figure 9 (a, b) Longitudinal sections through the fracture surface for a 371 °C (700 °F) tensile specimen of the cast material.

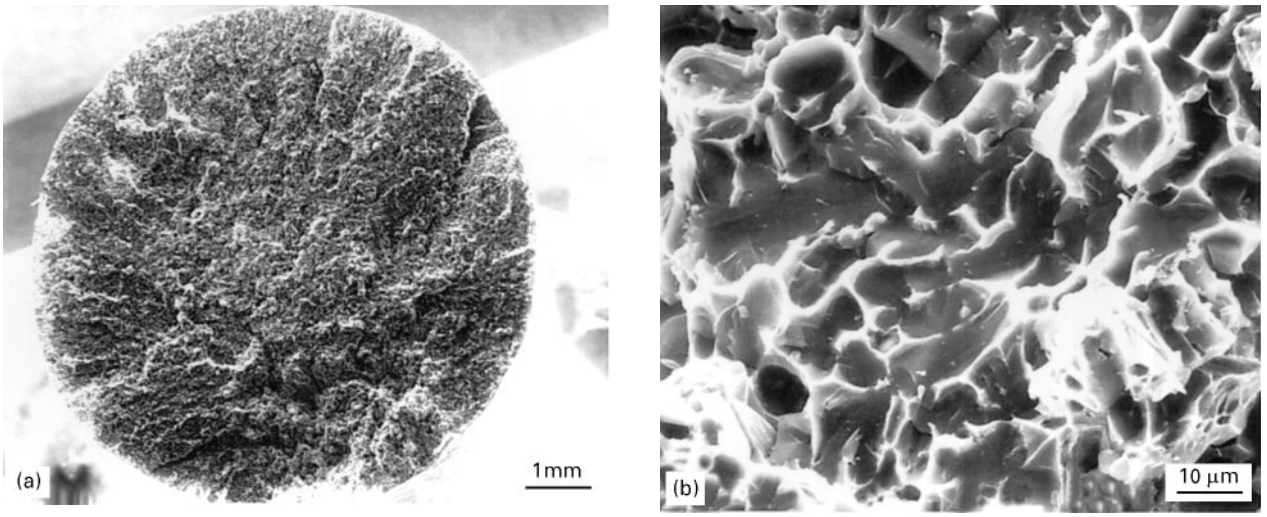

Figure 10 (a, b) SEM images of room-temperature tensile fracture surface of the extruded material.

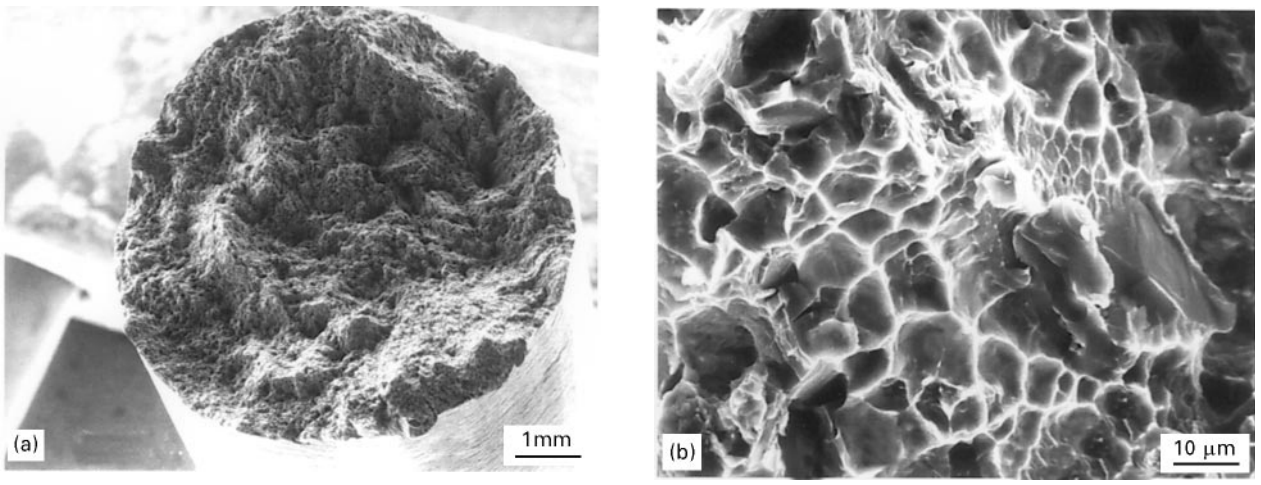

Figure 11 (a, b) SEM images of tensile fracture surface of the extruded material tested at 371 °C (700 °F).

For the extruded-material fracture surfaces shown in Figs 10 and 11, there is a gradual transition from a planar fracture surface at room temperature to a more undulating fracture surface at elevated temperature. This difference in fracture surface morphology is further illustrated by the longitudinal sections through the fracture surfaces shown in Figs 12 and 13. The higher magnification scanning electron micrograph for the room-temperature sample shows ductile ligaments of the aluminium regions extending above the more brittle beryllium regions that have failed by cleavage. At elevated temperature, these aluminium

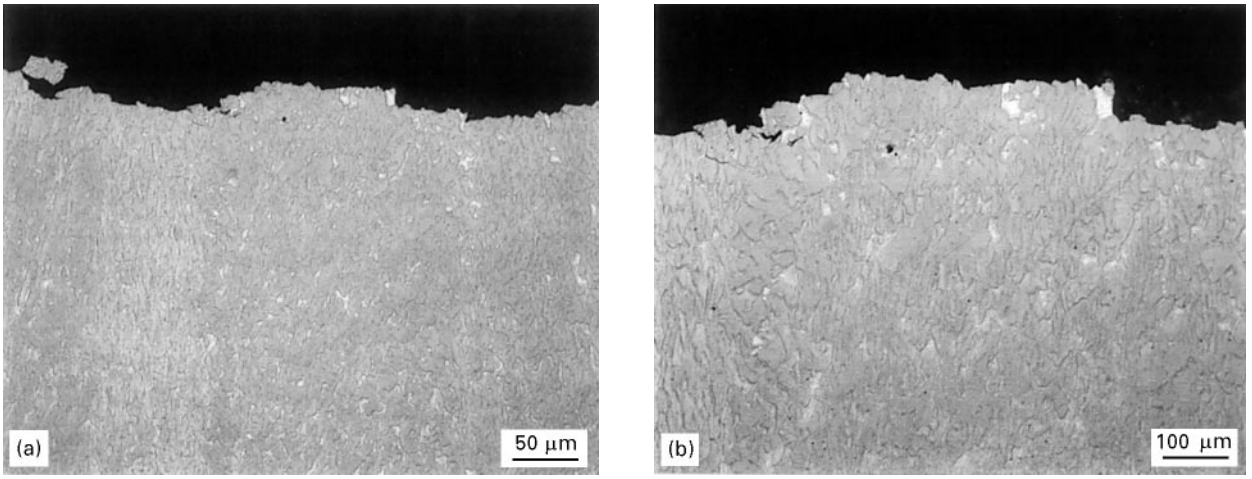

Figure 12 (a, b) Longitudinal section through the fracture surface for a room-temperature tensile specimen of the extruded material.

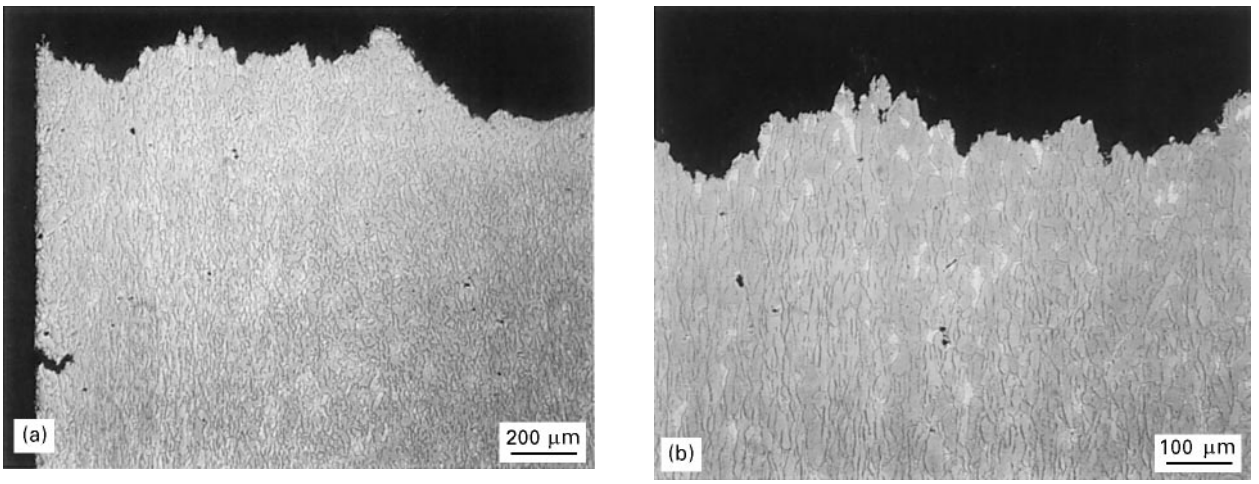

Figure 13 (a, b) Longitudinal sections through the fracture surface for a 371 °C (700 °F) tensile specimen of the extruded material.

regions extend to a greater degree above the planar beryllium regions and tend to dominate the fracture surface appearance.

3.2. Fatigue test results and failure analysis

The results of the fatigue testing are summarized in Table II and Fig. 14. The data for the wrought material falls consistently above that of the cast material. This result is consistent with respect to the relative tensile strength of the two materials. The $R = 0.1$, 232 °C (450 °F) 10^7 fatigue life appears to be approximately 172 MPa (25×10^3 p.s.i.) for the wrought material versus 69 MPa (10^4 p.s.i.) for the cast material.

TABLE II Fatigue test results for testing at 232 °C (450 °F) and an R value of 0.1

	Maximum stress		Cycles to failure ($\times 10^3$)
	(MPa)	(10^3 p.s.i.)	
Beralcast 363 – casting alloy	172	25	29.059
	138	20	1242.117
	104	15	3677.303
	69	10	>10 000
Beralcast 310 – wrought alloy	310	45	1.135
	276	40	69.959
	242	35	52.692
	242	35	699.514
	242	35	192.450
	207	30	1232.267

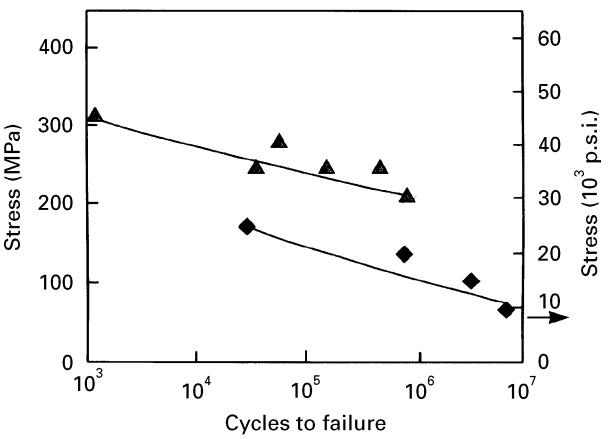

Figure 14 Fatigue data for the cast and extruded material: (◆) Beralcast 363, as cast; (▲) Beralcast 310, extruded. $R = 0.1$; 232 °C (450 °F).

Representative examples of the fatigue fracture surfaces for the two materials are shown in Figs 15 and 16. The fatigue fracture surfaces were very similar in appearance to the tensile fracture surfaces tested at

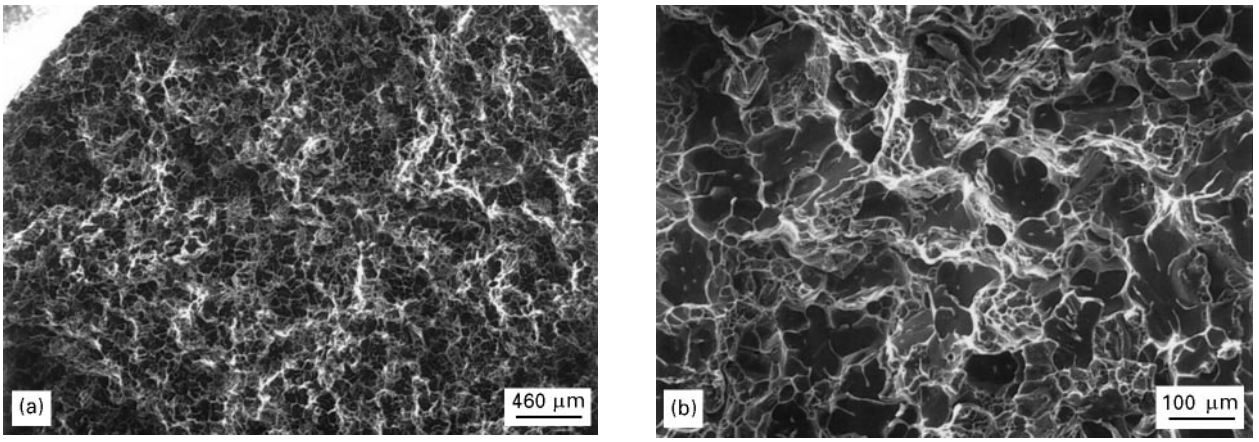

Figure 15 (a, b) SEM images of fatigue fracture surface of the cast material.

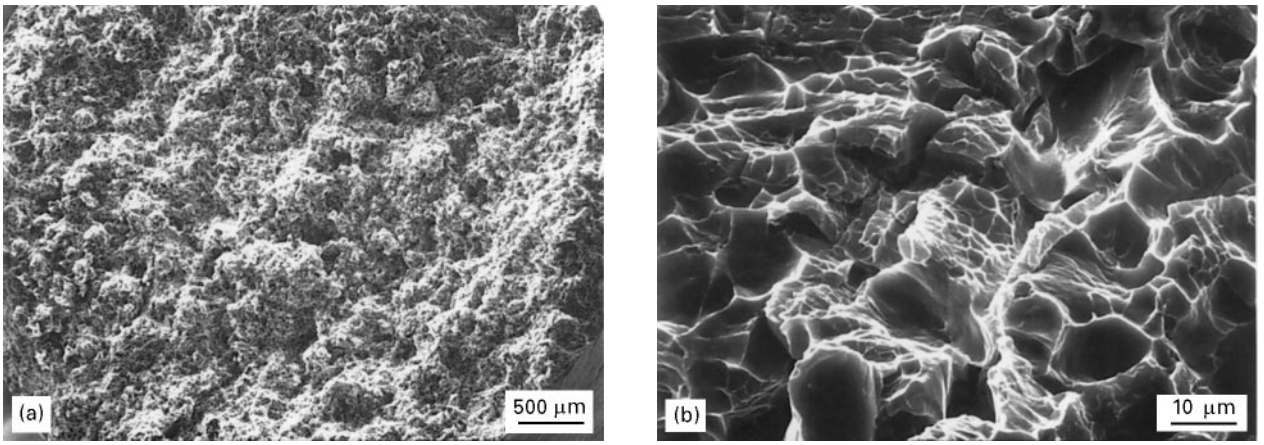

Figure 16 (a, b) SEM images of fatigue fracture surface of the extruded material.

the same temperature. There was no evidence of striations resulting from fatigue crack growth and there were no obvious fatigue initiation sites such as inclusions or porosity.

4. Discussion

4.1. Material stiffness levels

As mentioned in a companion paper that evaluates the mechanical properties of a powder metallurgy derived Be/Al material [2], it is worth noting the unique stiffness to density ratio that Be/Al materials possess. The measured room-temperature elastic modulus for the Beralcast alloys is about 228 GPa (33×10^6 p.s.i.), which is similar to the value of steels and nickel-base alloys. However, the density of the Beralcast 363 and 310 is only 2.12 g cm^{-3} (0.076 lb in^{-3}), which is about 20% lower than that of aluminium. From a stiffness/density ratio basis, the Beralcast materials are about a factor of 4.3 times higher than conventional metals such as steel, nickel, titanium and aluminium. This certainly suggests that the material is well suited for stiffness critical applications.

The data indicate that the room-temperature elastic modulus of the Beralcast materials was similar for both the wrought and the cast product. Because the Beralcast material essentially consists of pure beryllium regions that are embedded within an aluminium alloy matrix, one can analyse the properties of the material by treating it as a discontinuously reinforced metal. The modulus of a discontinuously reinforced material can be calculated using the following Tsai–Halpin equation [3].

$$E_c = E_m(1 + C_L n V_p)/(1 - n V_p) \quad (1)$$

where E_c is the composite modulus, E_m is the matrix modulus and V_p is the reinforcement volume fraction. The value of n is equal to

$$n = (E_r/E_m - 1)/(E_r/E_m + C_L) \quad (2)$$

where E_r is the modulus of the reinforcement. Finally, the value of C_L is dependent on geometric factors, which for a discontinuous reinforcement having an aspect ratio of s is

$$C_L = 2s + 40V_p^{10} \quad (3)$$

The appropriate values for Beralcast materials are $E_m = 69$ GPa (the modulus of aluminium), $E_r = 290$ GPa (the modulus of beryllium) and $V_f = 0.73$ (the volume fraction of beryllium).

The value for the aspect ratio of the beryllium regions was determined to be 8 for the wrought product, but is very difficult to define for the cast product. To span a range of values, the elastic modulus will be calculated assuming an aspect ratio of 2, 4, 8 and 12. The results of the calculations are reported in

TABLE III Calculated values for the elastic modulus of the Beralcast material as a function of beryllium region aspect ratio

Temp.		Be region aspect ratio	Calculated elastic modulus	
(°C)	(°F)		(GPa)	(10^6 p.s.i.)
Room temperature		2	212	30.7
		4	218	31.6
		8	223	32.3
		12	225	32.6
371	700	2	176	25.5
		4	183	26.5
		8	188	27.2
		12	190	27.5

Table III. The results indicate that the calculated elastic modulus is a weak function of the assumed particle aspect ratio, being about 221 GPa (32×10^6 p.s.i.). The calculated value is very similar to the observed results for both Beralcast materials. The good agreement between theory and experiment indicates that the bond existing between the beryllium and aluminium regions within the Beralcast materials is sufficient to permit effective load transfer from the aluminium to the stiffer beryllium. The net result is a material that behaves like a well-bonded discontinuously reinforced metal matrix composite.

The loss of modulus that occurs at elevated temperature should be considered with respect to the loss of modulus observed for monolithic aluminium and beryllium. Specifically, the modulus of aluminium at 371 °C (700 °F) has been reported to be about 52 GPa (7.5×10^6 p.s.i.) [4], while that of cross-rolled beryllium sheet has been reported to be about 248 GPa (36×10^6 p.s.i.) [5]. Substituting these elevated-temperature modulus values for E_m and E_r results in a calculated modulus value of about 186 GPa (27×10^6 p.s.i.) as reported in Table III. In this case, there is very good agreement between the calculated and the experimentally measured values for the wrought product, but the measured value for the cast product is lower than calculated. This lack of agreement for the cast product may be due to the difficulty in measuring the modulus value of a material having a very low yield strength, where plastic yielding makes it difficult to establish an extended linear region in the stress–strain curve. Sonic modulus measurements are more appropriate for such a situation.

4.2. Yield strength levels

The room-temperature yield strength of the Beralcast alloys is about 228 MPa (33×10^3 p.s.i.) for the casting alloy and about 297 MPa (43×10^3 p.s.i.) for the wrought alloy. Unfortunately, data do not exist on the yield strength levels for the aluminium alloy compositions used in the Beralcast materials. However, reasonable estimates can be made by performing microhardness testing on the aluminium regions of the casting alloy and by examining the strength levels of alloys with similar compositions. Note that because the alloying elements segregate preferentially to the aluminium alloy regions of the Beralcast materials and these regions constitute about one-third of the material, the weight per cent of the alloying elements in the aluminium alloy regions is about a factor of three higher than the overall nominal weight percentages reported in Section 2 above.

The microstructure of the Beralcast 363 material is sufficiently coarse to permit microhardness measurements to be made in the aluminium alloy regions. Prior work has established a correlation between Vickers microhardness (25 g load) and yield strength for 6061 Al [6]. Specifically, it was determined using a linear least squares fit (correlation coefficient of 0.98) the yield strength (YS, in MPa) was

$$\text{YS (MPa)} = -1.3 + 2.51\ \text{VH} \qquad (4)$$

where VH is the Vickers hardness level using a 25 g load. For the Beralcast 363 material, the Vickers hardness in the aluminium alloy regions was measured as 73. Therefore, the baseline strength of the aluminium alloy matrix for the Beralcast 363 material will be estimated to be 180 MPa (26×10^3 p.s.i.) for the discussion on strengthening mechanisms below. This is reasonably close to the experimentally measured Beralcast 363 yield strength of 228 MPa (33×10^3 p.s.i.).

The composition of the aluminium alloy regions for the wrought Beralcast 310 material is approximately Al–6Si–6Ag. The effect of silver on the strength of aluminium is not documented, but one can examine the properties of an Al–Si–Cu alloy as a reasonable estimate. (Copper and silver occupy the same column in the Periodic Table, and the Al–Cu and Al–Ag phase diagrams have similar features in the aluminium-rich region.) The commercial 308 Al alloy with a nominal composition of Al–5.5Si–4.5Cu, has a typical yield strength of 110 MPa (16×10^3 p.s.i.) in the F temper [7]. Additionally, the commercial 319 Al alloy with a nominal composition of Al–6Si–3.5Cu has a typical yield strength of 125 MPa (18×10^3 p.s.i.) in the F temper [7]. Therefore, the baseline strength of the aluminium alloy matrix for the Beralcast 310 material will be estimated to be 117 MPa (17×10^3 p.s.i.) for the discussion on strengthening mechanisms below.

To summarize with respect to yield strength levels, it appears that the Beralcast 363 casting alloy has similar strength levels to that of its aluminium alloy matrix. However, wrought Beralcast 310 alloy is substantially stronger than the estimated yield strength of its aluminium alloy matrix. Provided below is a discussion of candidate strengthening mechanisms to help explain these observations.

4.3. Dislocation-related strengthening mechanisms

Three distinct candidate strengthening mechanisms based on dislocation micromechanics will be considered as previously done in the strength analysis of dispersion-strengthened aluminium [8] and a companion paper on powder metallurgy Be/Al alloy [2]: the Orowan mechanism, grain-boundary strengthening (Hall–Petch strengthening) and an increase in dislocation density resulting from the relaxation of the

thermal expansion mismatch between the aluminium and beryllium phases. The equations and relevant data are repeated here for convenience.

For the Orowan mechanism, the particle by-passing stress, τ_c, is predicted to be [9]

$$\tau_c = \frac{1.13\,G\boldsymbol{b}}{2\pi D}\ln(d/r_0) \quad (5)$$

where G is the matrix shear modulus (28 GPa), $\boldsymbol{b}$ is the Burger's vector (0.286 nm), d is the average beryllium particle size, r_0 is the dislocation inner cut-off radius ($4\boldsymbol{b}$) and D is the average interparticle spacing (1 μm). The values utilized for d and D are typical values based on microstructural observations. For a polycrystalline fcc material, the projected yield strength increase from the Orowan mechanism is equal to $3\tau_c$.

The second mechanism to be considered is the grain-boundary strengthening mechanism. In this case, the strengthening increment, σ_{gb}, is calculated to be

$$\sigma_{gb} = K D_g^{-1/2} \quad (6)$$

where K is the Hall–Petch constant and D is the grain size. In this case, K will be taken to be 0.0725 MPa $m^{1/2}$ [8], while D_g will be assumed to be equal to the average interparticle spacing.

Finally, the strengthening increment, σ_d, resulting from an increase in dislocation density owing to the relaxation of thermal expansion mismatch stresses is equal to [10]

$$\sigma_d = A\,G\boldsymbol{b}\,\rho_{th}^{1/2} \quad (7)$$

where A is a constant equal to 1.25 for aluminium [11] and ρ_{th} is the density of dislocation loops punched out by particles of diameter d. Assuming full relaxation of the mismatch owing to the difference of thermal expansion coefficients, $\Delta\alpha$, for a temperature excursion, ΔT [10]

$$\rho_{th} = \frac{12\sqrt{2}\Delta\alpha\,\Delta T\,V_p}{\boldsymbol{b}\,d(1-V_p)} \quad (8)$$

For Beralcast materials, we assume that $\Delta\alpha$ is $3.6\times10^{-6}\,^{\circ}C^{-1}$ and a value for ΔT of 250 °C [8].

For the materials under consideration here, the two primary variables are the average particle size and the average interparticle spacing. Based on microstructural observations, the average particle diameter is 50 μm for Beralcast 363 and 15 μm for Beralcast 310. The average particle spacing is 25 μm for Beralcast 363 and 2 μm for Beralcast 310.

A summary of the calculated strengthening increments for each of the proposed dislocation-related strengthening mechanisms is provided in Table IV for both Beralcast materials. The results indicate the microstructure of the casting alloy is too coarse to result in appreciable strengthening from dislocation-based mechanisms. This is consistent with the measured Beralcast 363 yield strength being similar to that of its estimated *in situ* aluminium alloy matrix yield strength.

TABLE IV Calculated strengthening increments for dislocation based strengthening mechanisms

	Casting alloy Beralcast 363		Wrought alloy Beralcast 310	
	(MPa)	(10^3 p.s.i.)	(MPa)	(10^3 p.s.i.)
Orowan mechanism	2	0.3	20	2.9
Hall–Petch	15	2.1	51	7.4
Dislocation density	17	2.5	29	4.2
Total	34	4.9	100	14.5

For the wrought Beralcast 310 alloy, the baseline matrix strength as estimated above is 117 MPa (17×10^3 p.s.i.). The results in Table IV suggest that dislocation-related strengthening mechanisms can contribute an additional 100 MPa (14×10^3 p.s.i.) to the material yield strength, resulting in a net estimated yield strength level of 217 MPa (31×10^3 p.s.i.). In comparison, the experimentally determined yield strength for Beralcast 310 is 297 MPa (43×10^3 p.s.i.). These results suggest that additional strengthening mechanisms are operative in this material.

4.4. Continuum mechanics-related strengthening

The very high stiffness levels measured in the Beralcast materials indicate that load transfer in this system is effective. Therefore it is reasonable to consider whether load transfer from the aluminium to the beryllium can contribute to the observed strength level of the Beralcast materials. For short fibre/whisker-reinforced composites, the composite yield strength, σ_{cy}, due to load transfer is [12]

$$\sigma_{cy} = \sigma_{my}[0.5\,V_p(s+2) + (1-V_p)] \quad (9)$$

where σ_{my} is the matrix yield strength and s is the reinforcement aspect ratio.

For the Beralcast 363 material, the estimated in situ aluminium alloy region yield strength is 180 MPa (26×10^3 p.s.i.), but it is difficult to define an aspect ratio for the dendritic beryllium structure. Thus, the reinforcement shape assumptions inherent in Equation 8 may make it inappropriate for use to evaluate the Beralcast 363 material. To provide at least some indication of potential strengthening, it will be assumed that the beryllium aspect ratio is 1. Substituting an aspect ratio of 1 into Equation 8 results in a calculated strength level of $1.36\,\sigma_{my}$. Thus, the net strengthening increment is 65 MPa (9.4×10^3 p.s.i.) using a value of 180 MPa (26×10^3 p.s.i.) for σ_{my}. This result suggests that load transfer will not result in a substantial strengthening increment for the Beralcast 363 material.

For the Beralcast 310 material, the reinforcement aspect ratio is about 8 and the estimated *in situ* aluminium alloy region yield strength is 217 MPa (31×10^3 p.s.i.). Substituting these values into Equation 8 results in a calculated strength level of 850 MPa (123×10^3 p.s.i.). This calculated value is much higher than the observed value.

Note, however, the inherent assumption in Equation 8 that the beryllium regions are sufficiently strong to sustain the transferred load without yielding/fracturing. It is likely that the beryllium regions yield at moderate stress levels such that the calculated yield strength increment due to load transfer is not realized. By way of comparison, the yield strength observed for powder metallurgy based Be/Al material is about 545 MPa (79×10^3 p.s.i.). However, the typical diameter of the beryllium regions in the powder metallurgy material is 3 μm, compared to 15 μm for Beralcast 310. The much finer beryllium regions in the powder metallurgy material have higher strength relative to the beryllium regions of Beralcast 310, and therefore realize a greater strength increment due to load transfer prior to yielding/fracturing.

As a final comment, precise agreement between the measured and calculated yield strength values would be fortuitous because of the non-uniformity of the Beralcast microstructure. However, the calculations are very useful in terms of understanding the operative strengthening mechanisms. To summarize, it appears that strength of the Beralcast 363 casting alloy is controlled to a large extent by the strength of its aluminium alloy matrix. Limited additional strengthening occurs from the beryllium regions providing dislocation-based strengthening or strengthening due to load transfer. In contrast, the yield strength of the wrought Beralcast 310 alloy is substantially higher than that of its aluminium alloy matrix. Strengthening increments from both dislocation-based mechanisms and load transfer appear to be operative for this material.

4.5. Description of the tensile sample failure modes

Illustrations of the tensile fracture surfaces for cast material are shown in Figs 6–9. The appearance of the fracture surface for the cast material did not vary as a function of temperature. The fracture surfaces of the cast samples tend to have a relatively non-planar, rough morphology. Examination of longitudinal sections through the fracture surfaces, as provided in Figs 8 and 9, indicate that failure appears to be preferentially located in the aluminium regions of the alloy. Thus, failure appears to be controlled by failure of the aluminium regions or the Be/Al interfacial regions rather than the beryllium regions themselves. The tendency of the crack to follow the aluminium and Be/Al interfacial regions promote the non-planar topography of the fracture surface. The higher magnifications indicate that the aluminium regions fail by ductile dimple fracture, while the beryllium regions that do fail have a cleavage-type fracture.

For the extruded material fracture surfaces shown in Figs 10 and 11, there is a gradual transition from a planar fracture surface at room temperature to a more undulating fracture surface at elevated temperature. This difference in fracture surface morphology is further illustrated by the longitudinal sections through the fracture surfaces shown in Figs 12 and 13. At room temperature, Figs 10 and 12 show that the crack tends to propagate through both the aluminium and beryllium regions. The net result is a planar-type fracture surface morphology. In contrast, the elevated-temperature fracture surfaces shown in Figs 11 and 13 indicate that there is a tendency for preferential crack propagation in the aluminium and Be/Al interfacial regions. This latter effect tends to promote the transition to a non-planar type fracture surface morphology.

Finally, another feature should be noted in the lower magnification photograph of Fig. 13. This photograph shows a crack that has initiated at the surface of the samples away from the primary fracture surface. Multiple cracks were, in fact, observed around the circumference of failed tensile samples extending to distances of about 1 cm from the primary fracture surface. This feature was observed for only the higher ductility wrought product, and was present at both room and elevated temperature samples. This observation suggests that failure tends to initiate from the machined surface of the tensile samples.

4.6. Discussion of fatigue test results and failure analysis

The $R = 0.1$, 232 °C (450 °F) 10^7 fatigue life appears to be approximately 172 MPa (25×10^3 p.s.i.) for the wrought material and 69 MPa (10×10^3 p.s.i.) for the cast material. Unfortunately, data do not exist on the fatigue properties of beryllium produced by an ingot metallurgy route to allow for comparison. For both of the materials tested, however, the failure analysis does not indicate any obvious crack initiation site such as an inclusion or casting pore. Therefore, it is reasonable to assume that the materials are achieving their inherent fatigue-strength capability. The failure analysis also shows no evidence of striations as would be expected for controlled crack growth during the fatigue test. Rather, the lack of striations suggest that once a crack is initiated in the Beralcast material, failure occurs very soon thereafter by a tensile overload-type mechanism. In fact, for both materials, the appearance of the fatigue fracture surface was very similar to that of the tensile fracture surface at the same test temperature. There was one difference, however, for the wrought material, in that the fatigue specimens did not have any surface cracks present away from the primary fracture surface as reported above for the tensile samples.

5. Conclusion

The Beralcast materials were shown to have very high stiffness/density ratios relative to common structural materials. Because beryllium is insoluble in aluminium, discrete beryllium regions exist within the aluminium alloy matrices of the alloys. The net result is that the materials behave as discontinuous beryllium reinforced aluminium matrix composites. When the materials are treated as discontinuously reinforced composites, the measured stiffness levels

can be readily explained using standard composite theory. The wrought alloy was shown to have superior fatigue strength, tensile strength and ductility relative to the casting alloy, and also maintained a greater fraction of its tensile strength as a function of temperature.

The strength of the Beralcast 363 casting alloy is controlled to a large extent by the strength of its aluminium alloy matrix. Limited additional strengthening occurs from the beryllium regions contributing to dislocation-based strengthening or strengthening due to load transfer. In contrast, the yield strength of the wrought Beralcast 310 alloy is substantially higher than that of its aluminium alloy matrix. Strengthening increments from both dislocation-based mechanisms and load transfer appear to be operative for this material.

Fracture analysis revealed that failure of the casting alloy appears to be controlled by failure of the aluminium regions or the Be/Al interfacial regions rather than the beryllium regions themselves. The tendency of the crack to follow the aluminium and Be/Al interfacial regions promotes a non-planar topography of the fracture surface at room and elevated temperature. In contrast, the crack tends to propagate through both the aluminium and beryllium regions of the wrought alloy at room temperature, resulting in a planar-type fracture surface morphology. At elevated temperature, there is a tendency for preferential crack propagation in the aluminium and Be/Al interfacial regions and thus a transition to a non-planar type fracture surface morphology. For both Beralcast materials, the aluminium regions fail by ductile dimple fracture, while the beryllium regions that do fail have a cleavage-type fracture. Fracture analysis of fatigue samples reveal no obvious fracture initiation sites and no evidence of limited/controlled crack growth regions.

Acknowledgements

The support of this work by the Office of Naval Research and the Naval Air Warfare Center is gratefully acknowledged. The programme was jointly monitored by Dr Steve Fishman and Dr Gil London and their technical guidance during the performance of this work is appreciated.

References

1. W. T. NACHTRAB, K. R. RAFTERY and T. D. SANBORN, in "Proceedings of the 3rd Near Net Shape Manufacturing Conference", P. W. Lee and B. L. Ferguson (ASM International, Pittsburgh, PA, 1993) pp. 27–32.
2. V. C. NARDONE and T. J. GAROSSHEN, *J. Mater. Sci.*, submitted.
3. J. C. HALPIN, "Primer on Composite Materials: Analysis" (Technomic Publishing, Lancaster, PA, 1984) pp. 130–8.
4. R. F. WILDE and N. J. GRANT, "Dynamic Elastic Modulus Values at High Temperatures for Nickel-Base, Aluminium-Base and Metal-Metal Oxide Alloys", ASTM Proceedings, Vol. 57 (American Society for Testing and Materials, Philadelphia, PA, 1957) pp. 917–28.
5. "Designing with Beryllium" (Brush Wellman Inc., Cleveland, OH).
6. R. A. MAYOR, J. R. STRIFE and V. C. NARDONE, "Metal Matrix Composites Structural Data Development", AFWAL TR 86-4129 (1987).
7. "Metals Handbook", 9th Edn, Vol. 2, "Properties and Selection: Nonferrous Alloys and Pure Metals" (American Society for Metals, Metals Park, OH, 1979) pp. 159–60.
8. A. M. REDSTEN, E. M. KLIER, A. M. BROWN and D. C. DUNAND, *Mater. Sci. Eng.* **A201** (1995) 88.
9. M. F. ASHBY and A. S. ARGON (eds), "Physics of Strength and Plasticity" (Massachusetts Institute of Technology Press, Cambridge, MA, 1969) p. 113.
10. D. C. DUNAND and A. MORTENSEN, *Acta Metall. Mater.* **39** (1991) 127.
11. P. M. HAZZLEDINE, *Scripta Metall. Mater.* **26** (1992) 57.
12. V. C. NARDONE and K. M. PREWO, *ibid.* **20** (1986) 43.

Received 23 July
and accepted 23 October 1996